Hindawi Publishing Corporation
International Journal of Photoenergy
Volume 2009, Article ID 240402, 8 pages
doi:10.1155/2009/240402

Research Article

Hydrothermal Preparation of Gd^{3+}-Doped Titanate Nanotubes: Magnetic Properties and Photovoltaic Performance

Hoda S. Hafez,[1,2] M. Saif,[2,3] James T. McLeskey, Jr.,[4] M. S. A. Abdel-Mottaleb,[2] I. S. Yahia,[5] T. Story,[6] and W. Knoff[6]

[1] *Environmental Studies and Research Institute (ESRI), Minoufiya University, Sadat Branch, 32897 Sadat City, Egypt*
[2] *Nano-Photochemistry and Solarchemistry Laboratories, Department of Chemistry, Faculty of Science, Ain Shams University, Abbassia, 11566 Cairo, Egypt*
[3] *Department of Chemistry, Faculty of Education, Ain Shams University, Roxy, 32897 Cairo, Egypt*
[4] *Energy Conversion Systems Laboratory, Department of Mechanical Engineering, Virginia Commonwealth University, Richmond, VA 23284, USA*
[5] *Semi-Conductor Laboratory, Physics Department, Faculty of Education, Ain Shams University, Roxy, 32897 Cairo, Egypt*
[6] *Institute of Physics, Polish Academy of Sciences, Al. Lotnikow 32/46, 02-668 Warszawa, Poland*

Correspondence should be addressed to M. S. A. Abdel-Mottaleb, phochem08@photoenergy.org

Received 9 September 2009; Accepted 6 November 2009

Recommended by Frank Nüesch

Pure and Gd^{3+}-doped titanate nanotubes (TNTs) materials were synthesized by a hydrothermal method. Their morphology, optical properties, thermal stability, and magnetic properties were characterized by X-ray diffraction (XRD), transmission electron microscope (TEM), UV-Vis spectroscopy, thermal analysis, and magnetic measurements. It was found that doping renders Gd^{3+}-TNT visible light active and results in smaller crystallite size and larger surface area as well as higher thermal stability compared to pure titanate nanotubes. The estimated magnetic moments point to presence of weak antiferromagnetic interaction. Application of the prepared Gd^{3+}-TNT for modifying conventional photoanodes in polymer solar cells was attempted. Preliminary results show slightly improved photovoltaic energy conversion efficiency in the devices containing the newly designed Gd^{3+}-doped nanotubes.

1. Introduction

After the innovative work of Kasuga et al. [1], titanium dioxide and titanate nanotubes (TNTs) with large specific surface area and pore volume have gained promising and important prospect due to their fascinating microstructures and excellent properties [2]. TiO_2-derived nanotubes such as sodium titanate ($Na_xH_{1-x}Ti_3O_7$, $x \sim 0.75$) and hydrogen titanate ($H_2Ti_3O_7$ or $H_3Ti_5O_{11}$) prepared by a simple hydrothermal method are particularly interesting partly due to their one-dimensional nanostructures, uniform nanochannel, electronic conductivity, and larger specific surface area [3]. This showed promise for applications such as photocatalysis, sensing, adsorbents, mesoporous catalyst, and a good candidate material for dye-sensitized solar cells [4]. Nanotubes have a large specific surface area available for the absorption of photons compared to the bulk material while also providing channels for enhanced electron transfer, thereby helping to increase the efficiencies for photovoltaic energy conversion [5].

Rare earth ions have been widely used in high-performance luminescence devices, catalysts, and other functional materials because of the electronic, optical, and chemical characteristics originating from their 4f electrons [6]. Rare earth titanates have interesting dielectric, piezoelectric, and ferroelectric properties [7–9]. These materials usually possess a pyrochlore structure [10–13], which find numerous applications.

In this study, the titanate nanotubes doped with Gd^{3+} ions, with different concentrations of metal levels, were synthesized by hydrothermal treatment of pure anatase Gd^{3+}-doped TiO_2 powders in concentrated NaOH solution. It is the first time to obtain titanate nanotubes doped with paramagnetic Gd^{3+} ions in the view of their possible promising application in inorganic/polymer hybrid solar cell devices. Moreover, Gd^{3+} materials could be manipulated

with an external magnetic field for better alignment on different surfaces. The morphology, structure, thermal stability, and the magnetic properties of these titanate nanotubes doped with Gd^{3+} were described and discussed.

2. Experimental

2.1. Chemicals. Titanium(IV) isopropoxide, $Ti[O(C_3H_7)]_4$ (TTIP) 98.9%, Fluka, Gadolinium(III) nitrate pentahydrate $Gd(NO_3)_3 \cdot 5H_2O$ (99.9% pure grade), Aldrich, Sodium poly [2-(3-thienyl)-ethoxy-4-butylsulfonate], or PTEBS is a water-soluble thiophene polymer, American Dye Source. All other chemicals were of analytic purity grades and were used as received from Sigma-Aldrich Inc.

Conducting glass plates (FTO glass, Fluorine-doped tin oxide overlayer, and sheet resistance $25 \pm 5\,\Omega$, purchased from Hartford Glass Co., USA) were used as a substrate for precipitating titania porous film and were cut into $25 \times 25 \times 2.3$ mm sheets.

2.2. Synthesis of Gd^{3+}-Doped Titanate Nanotubes. The anatase Gd^{3+}-doped TiO_2 powders were first prepared by a conventional sol-gel process. 4.6 mL of TTIP is dissolved in 30 mL of methanol under stirring. This is followed by the addition of a mixture of 0.2 mL of concentrated HCl (catalyst), and 1.6 mL of water for hydrolysis. The hydrolysis of TTIP is allowed to proceed for 15–30 minutes. Then 0, 2, 5, 7 mol% of gadolinium nitrate dissolved in 20 mL of methanol is added to the above mixture under stirring. The resulting transparent colloidal suspension is stirred for 2 hours and aged for 24 hours until the formation of a gel. The resulting gel is dried at 80°C and then ground into a powder which is then calcinated at 450°C for 2 hours.

Gd^{3+}-doped titanate nanotubes (Gd^{3+}-TNTs) are prepared as described in Reference [14]. In a typical procedure, 100 mg of the pure anatase Gd^{3+}-doped TiO_2 nanoparticles are transferred into a Teflon-lined autoclave, which contained 20 mL of 10 M NaOH. The autoclave is then placed in an oven at 130°C for 48 hours. The contents of the autoclave are filtered and the resulting powders are washed with dilute HCl then deionized water until pH = 7 and dried at 80°C for 5 hours in a vacuum oven.

2.3. Material Characterizations. The nanotubes are characterized in a number of ways. Transmission Electron Microscopy (TEM) is done using a Jeol model JEM-1230 TEM operated at 100 kV. X-ray diffraction (XRD) analysis is made using a D/max γA. X-ray diffractometer (X′ Pert Pro, Japan) with Cu K_α radiation (K_α = 0.15418 nm) at 45 KV and 40 mA. Raman scattering spectra are recorded with a Horiba Jobin Yvon Raman spectrometer, using the 632.817 nm He-Ne laser for excitation. The light beam is focused through a standard Olympus Microscope with a 100 x lens down to 5–10 μm in diameter. Differential scanning calorimetry (DSC) and thermogravimetric analyses (TGA) are performed using a Perkin-Elmer PYRIS TGA, under N_2 gas, at a heating rate of 10°C/min. The temperature ranged from room temperature to 800°C in order to obtain crystallization and phase-transformation data. The optical properties of the samples are characterized by using a Jasco V550 UV-Vis spectrophotometer.

The dc magnetic susceptibility is carried out using superconducting SQUID magnetometry in the temperature range of 5–100 K with an excitation field $H_{ac} = 400$ Oe. On the basis that the magnetic susceptibility can be related to atomic properties, we converted mass magnetic susceptibility to the molar magnetic susceptibility χ_M using $\chi_M = \chi_g \cdot M_w$, where M_w is the molecular weight of the investigated samples.

For the characterization of the photovoltaic devices, current–voltage IV characteristics in the dark and under illumination were measured using a Keithley 236 source measurement unit with an AM 1.5 solar simulator (Spectra-Physics model 96000). The intensity of about 80 mW/cm^2 was measured with a Spectra-Physics optical power meter (model 407A).

2.4. Solar Cell Fabrication. The hybrid inorganic/polymer solar cell devices were fabricated as described in the literature [15] but with the addition of a TiO_2 hole blocking layer (HBL) [16]. Twelve devices were fabricated per substrate to check the reproducibility. Each device (area = 0.15 cm^2) consists of four layers on top of the FTO-coated glass substrate, namely, a dense TiO_2 HBL, a porous nanocrystalline TNT layer, the PTEBS polymer layer (approximately 8 μm thick) prepared by dropcasting, and Au layer deposited by sputter-coating.

The porous titanate layer was prepared by mixing 1 g titanate powder with 30 mL ethanol containing 1 mL acetic acid and five drops of triton X-100. The mixture was sonicated for 15 minutes and spin coated on top of the HBL at 2000 rpm for 30 s. The coating process was repeated to obtain thick films. The resulting films was sintered at 450°C for 2 hours in air.

3. Results and Discussion

3.1. Morphology and Crystal Properties. The TEM images of the precursor TiO_2 nanoparticles and the obtained undoped and Gd^{3+}-doped TNT after the hydrothermal treatment are shown in Figure 1. The pure titania precursor for the preparation of the titanate nanotubes were nanoparticles of pure anatase titania with an average diameter of about 15 nm as shown in Figure 1(a). The TEM morphologies of the undoped and Gd^{3+}-doped titanate nanotubes were shown in Figures 1(b) and 1(c). It is clear from these figures a well-identified multiwalled nanotubular structure with an average outer (inner) diameter of approximately 11 nm (5 nm) and a length of few hundreds of nanometers.

The mechanism for forming the nanotubes via the hydrothermal reaction was proposed by Viriya-Empikul et al. [17]. The process begins when the TiO_2 and doped TiO_2 powders are dissolved completely in the NaOH solution. These powders then form octahedrally configured $[Ti(OH)_6]^{2-}$ and $[M(OH)_6{}^{n-}]$ anions in the solution. The anions connect by sharing edges to form $Ti_5O_{11}{}^-$ nanosheets, which are a few thick atomic layers and they mayroll themselves into nanotubes to minimize the surface energy.

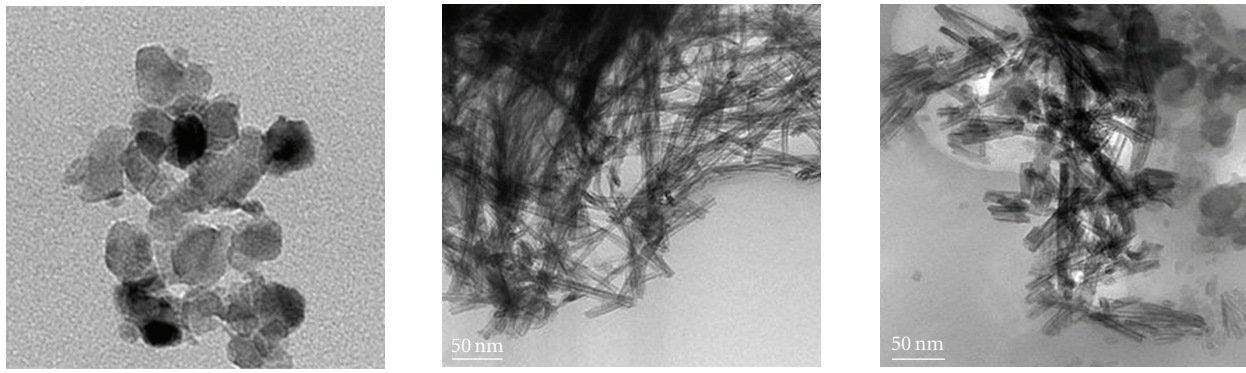

Figure 1: TEM micrographs of (a) TiO_2 nanoparticles, (b) pure TNT (c) 5% Gd^{3+}-TNT.

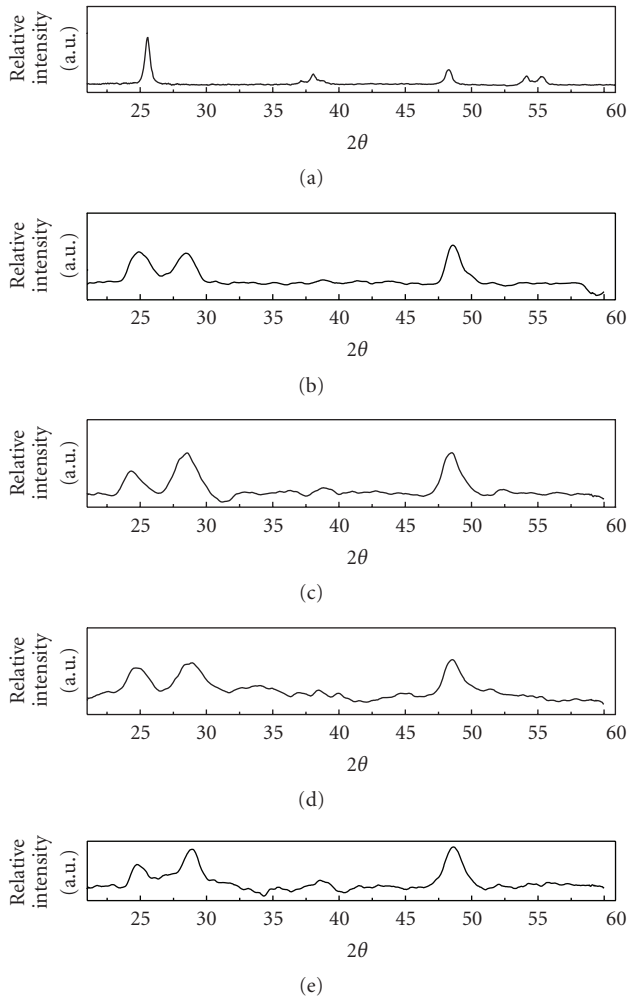

Figure 2: XRD patterns of: (a) Pure TiO_2; (b) pure TNT, and (c) 2% Gd^{3+}-TNT; (d) 5% Gd^{3+}-TNT; (e) and 7% Gd^{3+}-TNT.

XRD patterns of the starting precursor titania nanoparticles and hydrothermally synthesized Gd^{3+}-titanate nanotubes with different Gd^{3+}-doping level (from 2%–7% molar ratio) are presented in Figure 2. For the starting material (Figure 2(a)), only the peaks corresponding to the pure anatase TiO_2 phase (JCPDS 21-1272) were observed. However, the titanate nanotubes have a new crystalline structure which is different from the well-defined anatase and rutile phase, but compatible with the reported phase of known titanate (see Figure 2(b)) [18]. The peak positions of the pure and the Gd^{3+}-doped titanate nanotubes are almost the same and the obtained diffraction peaks are identified to be those of $H_3Ti_7O_{11}$ (JCPDS 44-0131) [19]. With enhancing the Gd^{3+}-doping level, it was found that there is no peak ascribed to gadolinia (Figures 2(c)–2(e)). It means that Gd^{3+} ions are indeed doped into the structure of titanate nanotubes and the doping of paramagnetic Gd^{3+} ions did not change the structure of nanotubes obviously [20].

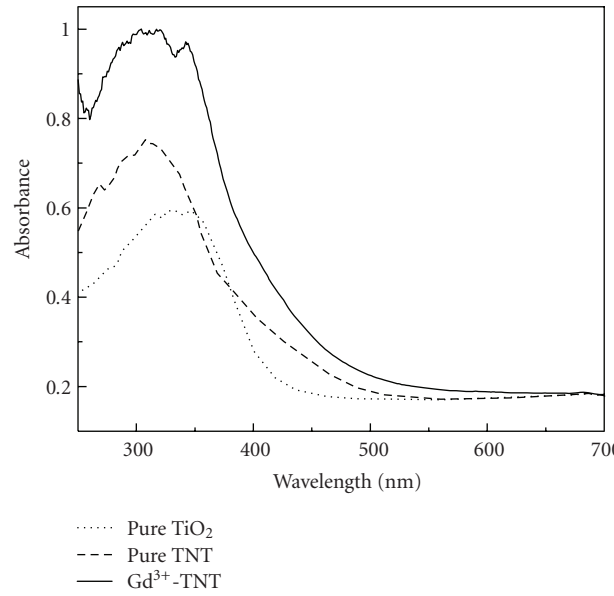

Figure 3: UV-Vis absorption spectra obtained from (1) pure TiO_2; (2) Pure TNT; (3) 5% Gd^{3+}-TNT.

3.2. Optical Properties. Figure 3 shows UV-Vis absorption spectra of the pure and Gd^{3+}-doped TNT compared with

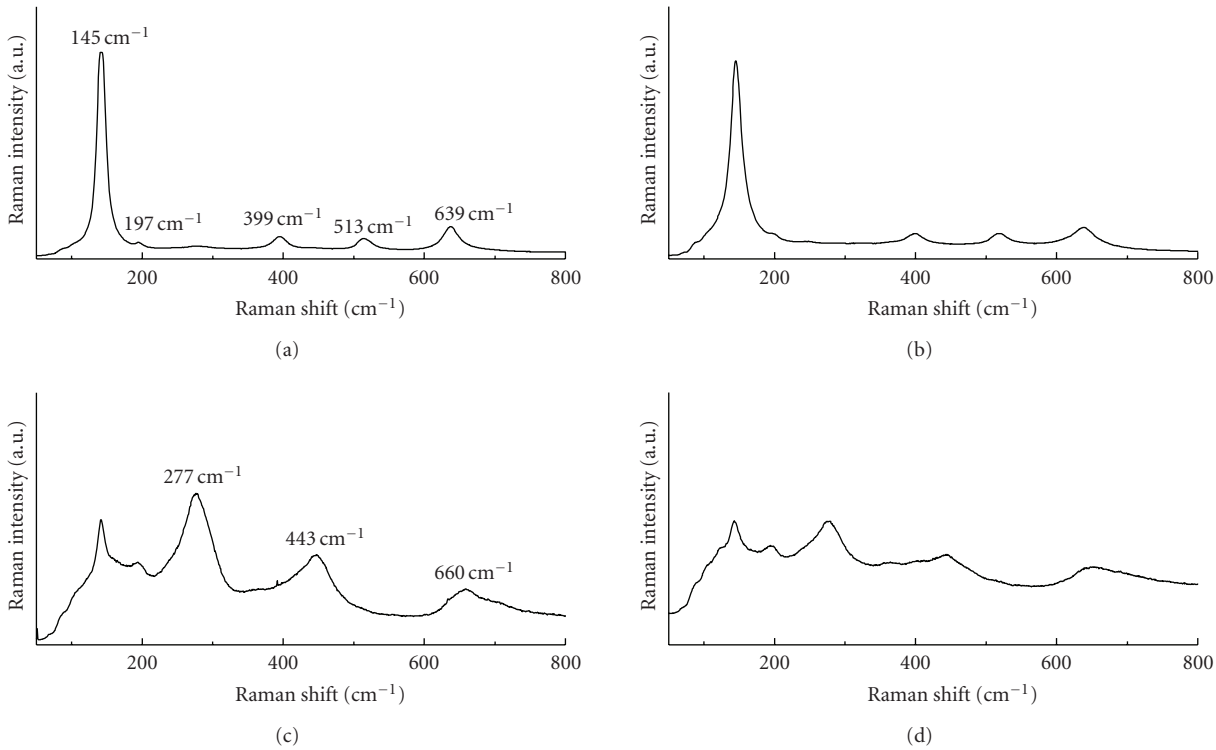

Figure 4: Raman spectra of: (a) Pure TiO_2; (b) 5% Gd^{3+}-TiO_2; (c) Pure TNT; (d) 5% Gd^{3+}-TNT.

pure titania nanoparticles. A red shift of the absorption onset is observed for the doped TNT relative to the bulk anatase TiO_2. The observed visible light activity could be attributed to the charge-transfer transition between the f electrons of Gd^{3+} with the conduction or valence band of titanate [21].

The Gd^{3+}-doped titanate nanotubes were further characterized by Raman spectra, which are shown in Figure 4. The pure TiO_2 anatase (Figure 4(a)) belongs to the symmetry space group D_{4h}^{19}. Group theory predicts six Raman active modes for the anatase phase: three E_g modes centered around 145, 197, and 639 cm^{-1}; two B_{1g} modes at 399 and 519 cm^{-1}; and an A_{1g} mode at 513 cm^{-1} [22]. In the Raman spectrum of 5% Gd^{3+}-doped anatase nanoparticles (see Figure 4(b)), all the observed Raman peaks were also identified from the tetragonal anatase phase. After forming nanotube structures, their Raman spectrum is apparently different from its precursor anatase phase. In Figures 4(c) and 4(d), there are three new peaks located at 277, 443 and 660 cm^{-1} in the Raman spectrum of the pure and Gd^{3+}-doped titanate nanotubes. The peak at 277 cm^{-1} is assigned to the characteristic phonon mode of titanate nanotubes [23]. The peak at 443 cm^{-1}, according to the study of Ma et al. [24], is assigned to the Ti–O bending vibration involving six-coordinated titanium atoms and three coordinated oxygen atoms. Based on the studies of Kasuga et al. [14], and Sun et al. [25], the peak at 660 cm^{-1} is due to the H-O-Ti vibration in titanate nanotubes [2]. From the Raman spectrum of Gd^{3+}-doped titanate nanotubes, the presence of any other vibration modes from secondary phases (e.g., Gadolinium oxides or various Gd^{3+}-Ti oxide species) was not detected for any of these spectra.

3.3. Thermal Analysis. Differential scanning calorimetry (DSC) and thermogravimetric analysis (TGA) of the as synthesized Gd^{3+}-TNT are performed to study the thermal stability of the obtained nanotubes over a high range of temperature with a heating rate of 10°C/min in nitrogen atmosphere from room temperature to 800°C. The TGA/DSC data of 5% Gd^{3+}-doped TNT are shown in Figure 5. There are three weight loss peaks at 110, 180 and 300°C, which is inconsistent with three peaks in DSC spectrum of the doped-titanate nanotubes. The different weight loss peaks corresponded to water of different states in titanate nanotubes, including dissociated H_2O molecular; physisorbed H_2O molecular; chemisorbed H_2O molecular and Ti–OH bonds within tubular structure [23]. No obvious exothermal or endothermal peaks were observed over the temperature range 300 to 600°C, suggesting that the nanotubes have good thermal stability. The TGA/DSC data of the other x% Gd^{3+}-doped TNT (not shown here) are identical to that of 5% Gd^{3+}-TNT.

3.4. Magnetic Properties. Temperature dependence of the magnetic susceptibility $\mathcal{X}$ of the paramagnetic materials shows a Curie Weiss type behavior which can be expressed as follows [26, 27]:

$$\chi_M = \mathcal{X}_{\text{diam.}} + \frac{C_M}{T - \theta_P}, \tag{1}$$

where χ_{diam} is the diamagnetic susceptibility of the host matrix, C_M is the molar Curie constant, θ_P is the paramagnetic Curie temperature, and T is the absolute temperature

Table 1: Magnetic parameters of xGd-(100-x) $H_2Ti_5O_{11}$ (x% Gd^{3+}-TNTs) where ($x = 2, 5, 7$).

X (mole % Gd)	θ_p, K, ± 0.04381	C_M, emu/mol, ± 0.17645	$\chi_{dia.}$, ± 0.00463	J, x10^{-3}	$\mu_{eff.}$, μ_B
2	-0.238	9.594	0.00054	24.86	6.19
5	-0.476	22.127	0.00467	21.53	6.16
7	-0.522	26.413	0.00026	19.77	5.49

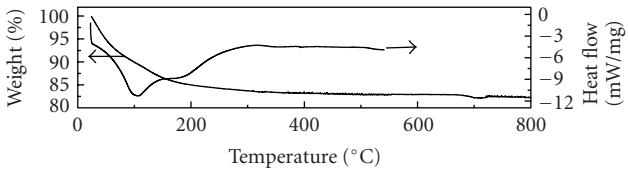

Figure 5: DSC and DTG data for the 5% Gd^{3+}-TNT.

in kelvins. The dc magnetic susceptibility results for $x Gd^{3+}$-(100-x)- $H_3Ti_7O_{11}$, where $x = 0$, 2, 5 and 7 nanotube are displayed in Figure 6(a) as a function of the temperature T. It is clear from this figure that with the increase of Gd^{3+} ions content, the magnetic susceptibility is increased. The pure TiO_2 shows the diamagnetic properties at the temperature higher than 20 K while x Gd^{3+}-(100-x)-$H_3Ti_7O_{11}$ that is, (x Gd^{3+}-(100-x) TNTs) where ($x = 2$, 5 and 7) showed a paramagnetic behavior. The data appear to follow a Curie–Weiss type behavior over the most of temperature range. All the measured curves are fitted according to the modified Curie Weiss law in the temperature range 5–100 K with a correlation coefficient around 0.9998. Values of the paramagnetic Curie temperature θ_P, are determined for the investigated samples and tabulated in Table 1. The magnitude of the paramagnetic Curie temperature θ_P increases with increasing the Gd^{3+} ions in the TNT matrix. Since the paramagnetic Curie temperature θ_P, is a rough measure of the strength of the interaction between the magnetic ions in the samples, the higher value implies stronger interaction and/or more ions participating in the interaction. The negative small value for the paramagnetic Curie temperatures indicates that the magnetic interaction is predominately antiferromagnetic in Gd^{3+}-doped TNT.

Figure 6(b) shows the magnetization versus the applied field curves (M versus H) of 2% Gd^{3+}-98 TNT (as a representative example) at 10 K. The almost linear field dependence of magnetization in this applied field range is a common feature of the paramagnetic compounds. Their fitting lines pass through the origin point indicating that Gd^{3+}-doped TNT is paramagnetic materials.

The experimental magnetic moment for the gadolinium ions $\mu_{Gd^{3+}}$ was calculated according to the following relation [28]:

$$\mu_{Gd^{+3}}(\exp.) = 2.827\sqrt{\frac{C_M}{x}}, \tag{2}$$

where x represents the molar fraction of Gd^{3+} inside the host matrix. The calculated values of the magnetic moment are given in Table 1. It is clear that the values of $\mu_{eff.}$ is less than the reported value of the atomic magnetic moment of Gd^{+3} ions in free ion state: $\mu_{Gd^{3+}} = 7.98\ \mu_B$ [29–31]. The small negative values of θ_P, $\theta_P < -2$ K suggest the presence of weak antiferromagnetic interaction. The assumption of the antiferromagnetic nature of the interaction between the Gd^{+3} ions is also supported by the fact that the effective magnetic moment per gadolinium ion, is less than the magnetic moment of the free gadolinium ion $\mu_{Gd^{3+}}$.

Based on the experimental data, one can also determine the molecular field constant J as follows [32]:

$$J = \left|\frac{\theta_P}{C_M}\right| = \frac{2zJ_{ij}}{N \cdot g^2 \cdot \mu_B^2}, \tag{3}$$

where N and Z are the total and exchange-coupled number of magnetic ions, J_{ij} is the magnetic exchange integral, g is their spectroscopic splitting factor and μ_B is the Bohr magnetron. The calculated values of $J = \theta_P/C_M$ from the experimental data are given in Table 1. It is clear that the molecular field theory is approximately constant with increasing the Gd^{3+} ions content. This behavior assumes that the ratio z/N is constant, the number of exchange-coupled Gd^{3+} ions being proportional to the total number of magnetic ions in the samples. The data above are consistent with a random distribution of Gd^{3+} ions. The magnetic properties of the materials are due to both isolated and exchange-coupled Gd^{3+} ions, their relative number being dependent on composition [30].

When a magnetic field is applied to a magnetic material, its magnetic moments tend to align themselves in the magnetic field direction and a more ordered state is achieved, so the magnetic entropy of the system decreases. In an isothermal process of magnetization, the magnetic entropy change of the system due to the application of a magnetic field, ΔS_M, can be derived from Maxwell relations in [27, 33]:

$$\Delta S_M(T, H) = \int_{H_{\min}}^{H_{\max}} \left(\frac{\partial M}{\partial T}\right)_H \cdot dH, \tag{4}$$

where $H_{\min}$ and $H_{\max}$ represent the initial and final values of the magnetic field. It seems clear that a high magneto-caloric effect will be observed when the temperature dependence of the magnetization (i.e., $\partial M/\partial T$) is large. This occurs, for example, at the Curie temperature for ferromagnetic-paramagnetic transitions, at which the maximum absolute value of the entropy change is expected, and at low temperatures for paramagnetic materials. Measurements of magnetic entropy variation when a fixed magnetic field change is applied allow one to determine whether a magnetic material may be considered to be a good magnetic refrigerant. Thus,

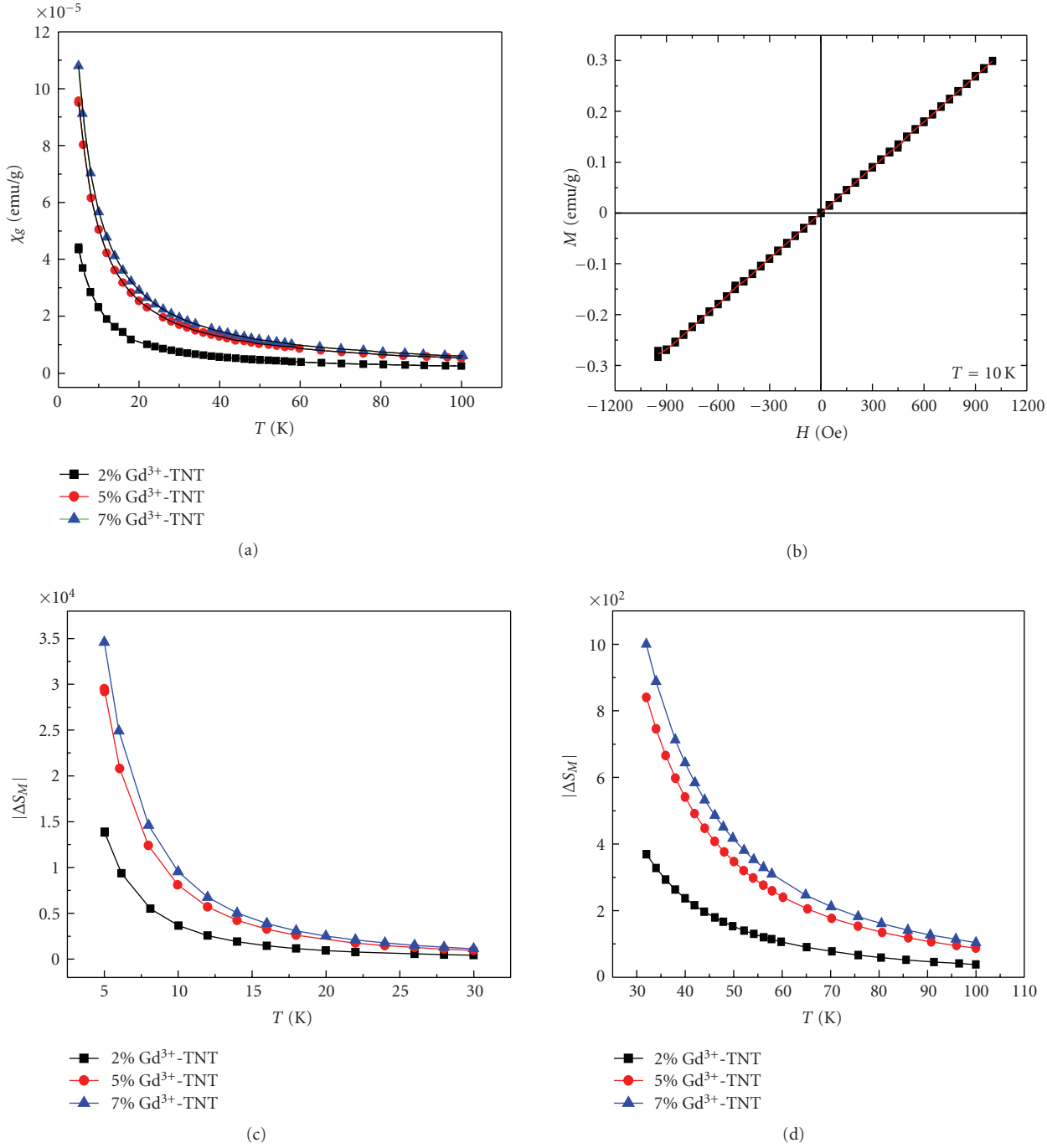

FIGURE 6: (a) dc magnetic susceptibility versus temperature for x Gd^{3+}-(100-x) TNT, where (x = 2, 5, 7); (b) The magnetization versus the applied field curves (M versus H) of 2% Gd^{3+}-98 TNT at 10 K (as a representative example); as well as (c) and (d) Temperature dependence of the entropy change for different mole percent of Gd^{3+}-TNT under an external magnetic field equal to 400 Oe.

for paramagnetic materials, the entropy change ΔS_M will be (5):

$$\Delta S_M = -\frac{C_M}{2}\frac{(\Delta H)^2}{\left(T-\theta_p\right)^2}, \tag{5}$$

where on has C_M in emu/mole, T and θ in K and ΔH in Oe. Figures 6(c) and 6(d) show the temperature dependence of the entropy change obtained for different mole percent of Gd^{3+} inside the host matrix TNT. It is clear that the entropy change decreases with increasing of the temperature and increased with increasing of the mole percent of Gd^{3+} ions added to the host materials. This behavior is expected for paramagnetic materials because their magnetization increases quickly when the temperature decreases at a low temperature range. Because of their paramagnetic behavior

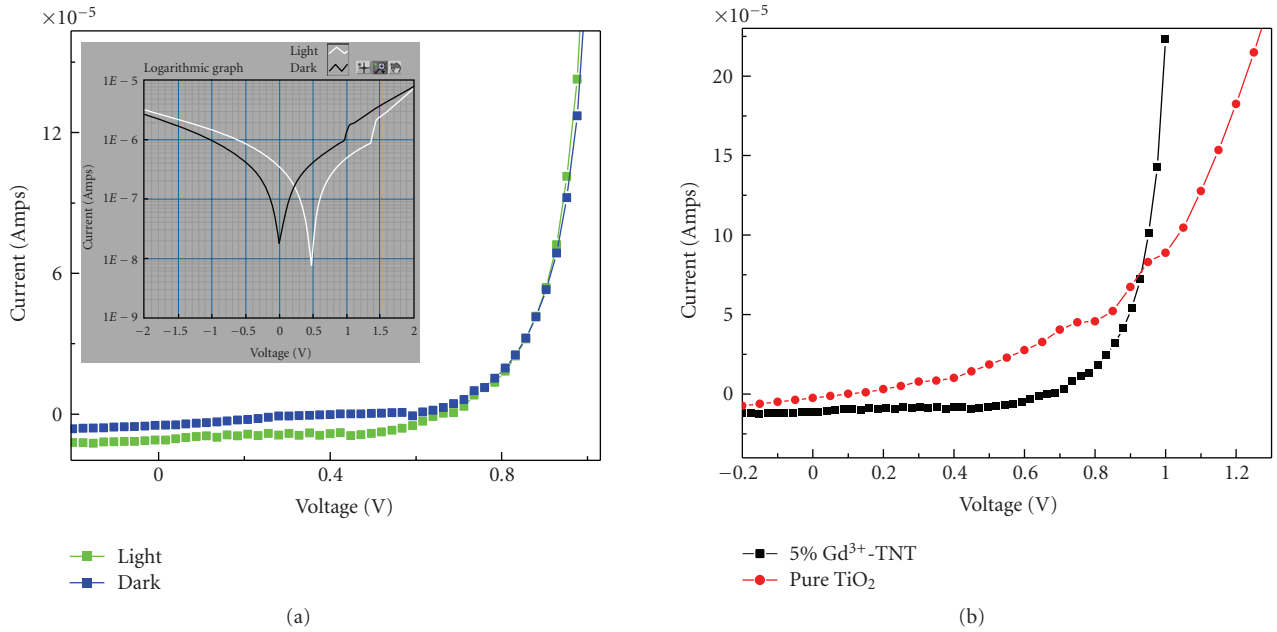

FIGURE 7: (a) Dark and Light IV curves of 5% Gd^{3+}-TNT/PTEBS hybrid polymer solar cell; (b) IV curves of pure TiO_2 and 5% Gd^{3+}-TNT hybrid solar cells.

at low temperatures, these materials have an entropy change that increases its absolute value when the temperature decreases. This implies the possibility of using these materials as active magnetic refrigerants in a wide range of temperature (5–100k).

3.5. Photovoltaic Efficiency of the Hybrid Polymer Solar Cells Based on Gd^{3+}-TNT. The hybrid polymer solar cells were fabricated by spin coating of the 5% Gd^{3+}-titanate nanotube layer onto the conductive FTO-glass which is repeated several times to obtain a thick film with approximately 8 μm. The titanate film was then sintered at 450°C for 30 minutes. The PTEBS polymer is then drop cast on top of the resulting nanotube layer. The photocurrent-voltage IV characterization of the obtained device is shown in Figure 7. Dark and light IV characteristics of the device were tested under AM1.5 illumination with an intensity of approximately 80 mW/cm^2 through the FTO electrode as shown in Figure 7(a). The PTEBS Gd^{3+}-doped TNT hybrid solar cell exhibits a short circuit current density (J_{sc}) of 84 μA/cm^2, an open circuit voltage (V_{oc}) of 0.66 V, and a fill factor (FF) of 0.49, resulting in a power conversion efficiency (η) of 0.034%. Comparing with the PTEBS pure titania devices (η = 0.01%), a slightly higher photovoltaic performance of Gd^{3+}-TNT polymer solar cell was observed as illustrated in Figure 7(b). This could be attributed to a better polymer loading and light harvesting of the applied titanate nanotube film.

These preliminary results demonstrate promising application of gadolinium doped titanate nanotubes for efficient hybrid polymer solar cells. Better alignment of the paramagnetic Gd^{3+}-TNT in polymer solar cell by applying external magnetic field is expected to enhance electron transport properties leading to more efficient light to electricity conversion. Further studies in this direction are in progress.

4. Conclusions

The aim has been to identify promising design for the future development of new multifunctional nanomaterials. We have successfully synthesized Gd^{3+}-TNT nanotubes through a simple hydrothermal procedure, and comprehensively characterized its properties. The structural and optical analyses indicate that doping of the TNT by Gd^{3+} enhances its thermal stability, hinders the growth of its crystallite size, and increases its surface area. Doped materials exhibit visible light absorption efficiency. Moreover, Gd^{3+}-TNT samples exhibit paramagnetic character and weak antiferromagnetic interaction. Testing the prepared hybrid polymer solar cells using doped 5% Gd^{3+}-TNT showed an improvement of light to electricity conversion efficiencies. There is still a need to optimize their alignment by external magnetic field manipulation to further improvement of the solar cells efficiency to a profitable exploitation extent.

Acknowledgments

This work is primarily funded by a grant from the US-Egypt Joint Science and Technology Board. Dr. Mona M. Saif and Dr. I.S. Yahia were supported under the Partnership and Ownership initiative (PAROWN) from the Egyptian Ministry of Higher Education. TEM microscopy was performed at VCU Department of Neurobiology & Anatomy microscopy facility. XRD measurements were made in the VCU Department of Chemistry.

References

[1] T. Kasuga, M. Hiramatsu, A. Hoson, T. Sekino, and K. Niihara, "Formation of titanium oxide nanotube," *Langmuir*, vol. 14, no. 12, pp. 3160–3163, 1998.

[2] Z. Tang, L. Zhou, L. Yang, and F. Wang, "A study on the structure transformation and luminescence of Eu(III) titanate nanotubes synthesized at various hydrothermal temperatures," *Journal of Alloys and Compounds*, vol. 481, no. 1-2, pp. 704–709, 2009.

[3] W. Wang, J. Zhang, H. Huang, Z. Wu, and Z. Zhang, "Surface-modification and characterization of H-titanate nanotube," *Colloids and Surfaces A*, vol. 317, no. 1–3, pp. 270–276, 2008.

[4] M. Adachi, Y. Murata, I. Okada, and S. Yoshikawa, "Formation of titania nanotubes and applications for dye-sensitized solar cells," *Journal of the Electrochemical Society*, vol. 150, no. 8, pp. G488–G493, 2003.

[5] K. Uchiyama, M. Yoshida, Y. Hayashi, and K. Narasaka, "Synthesis of dihydropyrroles and tetrahydropyridines by the intramolecular cyclization of O-methylsulfonyloximes having an active methine group," *Chemistry Letters*, no. 7, pp. 607–608, 1998.

[6] L. Fu, Z. Liu, Y. Liu, et al., "Coating carbon nanotubes with rare earth oxide multiwalled nanotubes," *Advanced Materials*, vol. 16, no. 4, pp. 350–352, 2004.

[7] I. Burn and S. Neirman, "Dielectric properties of donor-doped polycrystalline $SrTiO_3$," *Journal of Materials Science*, vol. 17, no. 12, pp. 3510–3524, 1982.

[8] D. W. Hwang, J. S. Lee, W. Li, and S. H. Oh, "Electronic band structure and photocatalytic activity of $Ln_2Ti_2O_7$ (Ln = La, Pr, Nd)," *Journal of Physical Chemistry B*, vol. 107, no. 21, pp. 4963–4970, 2003.

[9] M. A. Subramanian, G. Aravamudan, and G. V. Subba Rao, "Oxide pyrochlores—a review," *Progress in Solid State Chemistry*, vol. 15, no. 2, pp. 55–143, 1983.

[10] K. B. Helean, S. V. Ushakov, C. E. Brown, et al., "Formation enthalpies of rare earth titanate pyrochlores," *Journal of Solid State Chemistry*, vol. 177, no. 6, pp. 1858–1866, 2004.

[11] F. X. Zhang and S. K. Saxena, "Structural changes and pressure-induced amorphization in rare earth titanates $RE_2Ti_2O_7$ (RE: Gd, Sm) with pyrochlore structure," *Chemical Physics Letters*, vol. 413, no. 1–3, pp. 248–251, 2005.

[12] N. Zhong, P. H. Xiang, D. Z. Sun, and X. L. Dong, "Effect of rare earth additives on the microstructure and dielectric properties of $0.67Pb(Mg_{1/3}Nb_{2/3})O_3 - 0.33PbTiO_3$ ceramics," *Materials Science and Engineering B*, vol. 116, no. 2, pp. 140–145, 2005.

[13] S. T. Bramwell, M. N. Field, M. J. Harris, and I. P. Parkin, "Bulk magnetization of the heavy rare earth titanate pyrochlores—a series of model frustrated magnets," *Journal of Physics: Condensed Matter*, vol. 12, no. 4, pp. 483–495, 2000.

[14] T. Kasuga, M. Hiramatsu, A. Hoson, T. Sekino, and K. Niihara, "Titania nanotubes prepared by chemical processing," *Advanced Materials*, vol. 11, no. 15, pp. 1307–1311, 1999.

[15] Q. Qiao and J. T. McLeskey Jr., "Water-soluble polythiophene-nanocrystalline TiO_2 solar cells," *Applied Physics Letters*, vol. 86, no. 15, Article ID 153501, 3 pages, 2005.

[16] P. Ravirajan, D. D. C. Bradley, J. Nelson, et al., "Efficient charge collection in hybrid polymer/ TiO_2 solar cells using poly(ethylenedioxythiophene)/polystyrene sulphonate as hole collector," *Applied Physics Letters*, vol. 86, no. 14, Article ID 143101, 3 pages, 2005.

[17] N. Viriya-Empikul, N. Sano, T. Charinpanitkul, T. Kikuchi, and W. Tanthapanichakoon, "A step towards length control of titanate nanotubes using hydrothermal reaction with sonication pretreatment," *Nanotechnology*, vol. 19, no. 3, Article ID 035601, 6 pages, 2008.

[18] Q. Chen, W. Zhou, G. H. Du, and L.-M. Peng, "Trititanate nanotubes made via a single alkali treatment," *Advanced Materials*, vol. 14, no. 17, pp. 1208–1211, 2002.

[19] *JCPDS PDF-2 Release 2001*, ICDD, Newtown Square, Pa, USA, 2001.

[20] M. Wang, G. Song, J. Li, L. Miao, and B. Zhang, "Direct hydrothermal synthesis and magnetic property of titanate nanotubes doped magnetic metal ions," *Journal of University of Science and Technology Beijing: Mineral Metallurgy Materials*, vol. 15, no. 5, pp. 644–648, 2008.

[21] W. Zhou, Y. Zhou, and S. Tang, "Formation of TiO_2 nano-fiber doped with Gd^{3+} and its photocatalytic activity," *Materials Letters*, vol. 59, no. 24-25, pp. 3115–3118, 2005.

[22] M. Mikami, S. Nakamura, O. Kitao, and H. Arakawa, "Lattice dynamics and dielectric properties of TiO_2 anatase: a first-principles study," *Physical Review B*, vol. 66, no. 15, Article ID 10.1103/PhysRevB.66.155213, 6 pages, 2002.

[23] L. Qian, Z.-L. Du, S.-Y. Yang, and Z.-S. Jin, "Raman study of titania nanotube by soft chemical process," *Journal of Molecular Structure*, vol. 749, no. 1–3, pp. 103–107, 2005.

[24] R. Ma, K. Fukuda, T. Sasaki, M. Osada, and Y. Bando, "Structural features of titanate nanotubes/nanobelts revealed by raman, X-ray absorption fine structure and electron diffraction characterizations," *Journal of Physical Chemistry B*, vol. 109, no. 13, pp. 6210–6214, 2005.

[25] X. Sun and Y. Li, "Synthesis and characterization of ion-exchangeable titanate nanotubes," *Chemistry: A European Journal*, vol. 9, no. 10, pp. 2229–2238, 2003.

[26] M. A. Salim, G. D. Khattak, P. S. Fodor, and L. E. Wenger, "X-ray photoelectron spectroscopy (XPS) and magnetization studies of iron-vanadium phosphate glasses," *Journal of Non-Crystalline Solids*, vol. 289, no. 1–3, pp. 185–195, 2001.

[27] A. Fernández, X. Bohigas, J. Tejada, E. A. Sulyanova, I. I. Buchinskaya, and B. P. Sobolev, "The magnetocaloric effect in high-spin paramagnetic rare-earth fluorites," *Materials Chemistry and Physics*, vol. 105, no. 1, pp. 62–66, 2007.

[28] S. Simon, I. Ardelean, S. Filip, I. Bratu, and I. Cosma, "Structure and magnetic properties of Bi_2O_3-GdO_2-Gd_2O_3 glasses," *Solid State Communications*, vol. 116, no. 2, pp. 83–86, 2000.

[29] I. Coroiu, E. Culea, I. Vida Simiti, and A. Darabont, "Magnetic properties of some gadolinium silica glass ceramics," *Journal of Optoelectronics and Advanced Materials*, vol. 8, no. 2, pp. 526–528, 2006.

[30] I. Ardelean and L. Griguta, "EPR and magnetic susceptibility studies of B_2O_3-Bi_2O_3-Gd_2O_3 glasses," *Journal of Non-Crystalline Solids*, vol. 353, no. 24-25, pp. 2363–2366, 2007.

[31] Y. B. Saddeek, I. S. Yahia, W. Dobrowolski, L. Kilanski, N. Romčević, and M. Arciszewska, "Infrared, raman spectroscopy and ac magnetic susceptibility of Gd_2O_3-TeO_2-V_2O_5 glasses," *Optoelectronics and Advanced Materials-Rapid Communications*, vol. 3, pp. 559–564, 2009.

[32] L. F. Bates, *Modern Magnetism*, Cambridge University, London, UK, 1962.

[33] A. M. Tishin and Y. I. Spichkin, *The Magnetocaloric Effect and Its Applications*, chapter 1, Institute of Physics Publishing, Bristol, UK, 2003.